PAPER

Check for updates

Conversion of C_8 aromatics over a dual-bed catalyst

Peixi Feng, [ID] Chenglin Kang,* Zhenhuan Zhou, Xin Yue, Zhongxun Liu, Yueting Gai, Junjun Shi and Baoning Zong [ID]

A dual-bed catalyst was prepared for the conversion of C_8 aromatics. The upper bed layer consisted of ZSM-5 covered with SiO_2, primarily utilized for ethylbenzene dealkylation. By employing tetraethyl orthosilicate (TEOS) as a deposition agent through the chemical liquid deposition (CLD) method, the modified ZSM-5 catalyst exhibited optimal catalytic performance at a TEOS addition of 0.6 g per gram of catalyst. The lower bed layer contained ZSM-39 catalyst, mainly employed for xylene isomerization reaction. ZSM-39 was synthesized using pyrrolidine as the template, and the best catalytic performance was achieved when the OH^-/SiO_2 molar ratio in the synthesis system was 0.05. The mass ratio between the upper and lower agents was maintained at 1 : 1. Compared to traditional single-bed ZSM-5 catalysts, the dual-bed catalyst demonstrated enhanced activity and selectivity.

Introduction

para-Xylene (PX) is a crucial organic chemical raw material, commonly used in the production of terephthalic acid, which serves as a precursor for polyester production and is of substantial demand.[1–3] Xylene isomerization plays a vital role in PX production by converting less significant *o*-xylene(OX) and *m*-xylene(MX) into PX.[4–6] The xylene isomerization unit typically receives lean PX feed from the adsorption separation unit, which usually contains approximately (4–10) wt% ethylbenzene (EB).[7,8] Due to the narrow boiling point difference of only 0.8 °C between EB and PX, the presence of EB significantly complicates the purification process of PX.[9] Consequently, it becomes necessary to treat this portion of EB within the xylene isomerization unit through deethylation as a typical approach.[10–12] Therefore, primary reactions occurring in the xylene isomerization unit involve interconversion among three xylene isomers and deethylation of EB.[13–15] Additionally, side reactions such as xylene disproportionation and transalkylation between xylenes and EB occur, which leads to lower total yield of xylenes compared to that of reactant.[16,17]

All of the above reactions in the xylene isomerization process are catalyzed by Brønsted acid,[18–20] thus zeolite catalysts, particularly ZSM-5, are commonly employed in this process.[21–23] To mitigate catalyst deactivation caused by ethylene formation during the deethylation of ethylbenzene, minute amounts of noble metals are typically impregnated onto the catalyst and hydrogen gas is introduced to saturate the ethylene, thereby enhancing the longevity of the catalyst.[24–26] The conventional

xylene isomerization process employs a single-bed catalyst, where the entire bed consists of uniform catalysts of only one type. Some researchers have developed a dual-bed xylene isomerization catalyst, which divides the catalyst bed into two layers. The upper layer primarily facilitates ethylbenzene deethylation reaction, while the lower layer promotes xylene isomerization reaction. In comparison to the single-bed process, the dual-bed approach achieves higher EB conversion and xylene yield, indicating enhanced activity and selectivity.[27,28] The upper catalyst passivates the acid center on the outer surface of zeolite through surface loading SiO_2, thereby selectively facilitating deethylation of ethylbenzene exclusively within the zeolite pore channel. There are two primary approaches for loading SiO_2 onto the surface of zeolite. One approach involves synthesizing a thin and uniform layer of silicate-1 zeolite film on the surface, resulting in a core–shell zeolite structure.[29,30] The surface film synthesized by this method exhibits exceptional thinness and uniformity, however, this method requires a more complex synthesis process and prolonged preparation time.[31] The other approach entails depositing inert silica on the zeolite surface using silicification reagents such as $SiCl_4$, silicone oil, or tetraethyl orthosilicate (TEOS) through chemical vapor deposition (CVD) or chemical liquid deposition (CLD) methods.[32,33] Manstein *et al.* employed the CVD technique and utilized TEOS as a silicification agent for depositing SiO_2 onto the surface of ZSM-5. They observed that temperature significantly influenced the rate of deposition, with excessively high temperatures resulting in overly rapid deposition rates, leading uneven surface coverage and difficulties in controlling the amount deposited. Consequently, it was necessary to perform repeated depositions at lower temperatures.[34] Yue *et al.* employed the CLD method and utilize $SiCl_4$ as

Research Institute of Petroleum Processing, SINOPEC, Beijing, 100083, PR China. E-mail: kangcl.ripp@sinopec.com

silicification reagents for depositing SiO$_2$ onto the surface of ZSM-5. It was observed that precise control over pore size adjustment could be achieved by varying the concentration of deposited agent, while preserving the internal structure of zeolite pores intact. The modified zeolite exhibits excellent shape selectivity performance.[35] In comparison to CVD, the CLD method offers greater operational ease and enhanced control over the deposition quantity of SiO$_2$, thereby presenting promising prospects for practical applications.[36]

The high silicon zeolite ZSM-39, characterized by the MTN structure code, was initially synthesized in the 1980s by Mobil Company.[37–39] The structure of ZSM-39 zeolite was thoroughly investigated by Schlenker, revealing the presence of five- and six-membered rings. Consequently, its pore size is sufficiently restricted to prohibit the ingress of organic molecules containing benzene rings.[40] ZSM-39 zeolite can be synthesized hydrothermally using pyrrolidine, propylamine, and tetramethylammonium bromide as template agents.[41,42] Due to its narrow pores, ZSM-39 zeolite has limited applications and is primarily used in lubricating oil hydrotreatment.[43] Nevertheless, recent research has demonstrated that ZSM-39 exhibits remarkable selectivity in catalyzing xylene isomerization. Therefore, ZSM-39 was selected as the lower layer catalyst here.

In this work, a dual-bed catalyst was prepared for the conversion of C$_8$ aromatics. The upper bed catalyst utilized ZSM-5 zeolite with surface modification achieved by depositing SiO$_2$ through CLD using TEOS as the deposition agent. The influence of TEOS concentration on the deposition process was investigated. The lower bed catalyst utilized ZSM-39 which was synthesized using pyrrolidine as a SDA. Compared to traditional single-layer ZSM-5 zeolite catalysts, the dual-bed catalyst exhibited enhanced activity and selectivity.

Experimental

Synthesis of ZSM-5

0.328 g NaAlO$_2$ (Ar), 0.64 g NaOH (Ar), 59.75 g deionized water, 8.42 g TEAOH (35 wt% in water) were mixed for 1 h. Then, 12 g fumed silica was added into the mixture gradually under continuous stirring and aged for 2 h. The molar ratio of the mixture was $20H_2O : 0.1TEAOH : 0.05Na_2O : 0.01Al_2O_3 : SiO_2$. The mixture was then transferred into a teflon-lined autoclave and hydrothermally treated at 170 °C for 30 h. The product was filtered and washed with deionized water until the filtrate was neutral, dried at 120 °C for 6 h, calcined at 550 °C for 6 h to obtain NaZSM-5. Ion exchange was carried out in 1 mol L^{-1} NH$_4$Cl solution at 70 °C, then filtered, washed and dried. HZSM-5 was obtained after calcined at 500 °C for 6 h. The ZSM-5 sample was denoted as Z5.

CLD deposition modification of ZSM-5

The HZSM-5 zeolite was compressed and pulverized, and particles with a size of 20–40 mesh were selected for CLD modification. 10 g catalyst was mixed with 30 mL cyclohexane, followed by the addition of 6 mL TEOS, and continuously shaken at 50 °C for 7 h. Subsequently, the catalyst was filtered and washed with ethanol to remove excess TEOS, and then washed with deionized water. Dried at 120 °C for 6 h, calcined at 550 °C for 6 h. The influence of TEOS concentration on modification results was investigated by varying the amount of added TEOS to 2 mL, 4 mL and 8 mL. The resulting catalyst was denoted as Z5-S-x, where x represents the volume of TEOS added per gram of catalyst which was 0.2 mL g^{-1}, 0.4 mL g^{-1}, 0.6 mL g^{-1} and 0.8 mL g^{-1} respectively.

Synthesis of ZSM-39

0.3 g NaOH, 1.07 g pyrrolidine(PY, Ar), 53.95 g deionized water were mixed for 0.5 h, 0.207 g pseudo boehmite(AlOOH, 70% wt Al$_2$O$_3$) was added to the mixture and stirred for 1 h. Then 9 g fumed silica was added gradually under continuous stirring, the resulting mixture was aged for 2 h. The molar ratio of the mixture was $20H_2O : 0.1PY : 0.05OH^- : 0.01Al_2O_3 : SiO_2$. The mixture was transferred into a Teflon-lined autoclave and hydrothermally treated at 180 °C for 96 hours. The product is filtered and washed with deionized water until the filtrate is neutral, dried at 120 °C for 6 h, calcined at 550 °C for 6 h to obtain NaZSM-39. Ion exchange was carried out in 1 mol per L NH$_4$Cl solution at 70 °C, then filtered, washed and dried. HZSM-39 was obtained after calcined at 500 °C for 6 h. In order to investigate the influence of OH$^-$/SiO$_2$ on zeolite structure, the OH$^-$/SiO$_2$ molar ratio in the synthetic system was varied to 0.01, 0.03, and 0.07 by adjusting the amount of NaOH added. The resulting zeolite samples were denoted as PY-x, where x represents the corresponding OH$^-$/SiO$_2$ molar ratio which was 0.01, 0.03, 0.05 and 0.07 respectively.

Catalyst characterizations

XRD patterns were obtained on a rikagu D/MAX-IIIA with Cu kα radiation, the operating voltage is 40 kV and current is 40 mA. The pore volume and the specific surface area were tested by nitrogen adsorption measurements at −196 °C on a Micromeritics ASAP 2020. Each sample was evacuated for 8 h at 350 °C before tested. The total surface area was calculated by BET equation, and the total pore volume was determined at $p/p_0 = 0.99$. The micropore surface area and the micropore volume were calculated by the t-plot method. The scanning electron microscope (SEM) images were taken on the Hitachi SU-8010, the operating voltage was 5 kV. The bulk elemental of samples were analyed using X-ray fluorescence (XRF) on a Rigaku ZSX100E X-ray fluorescence spectrometer instrument, and the surface elemental of samples were analyed by X-ray photoelectron spectroscopy (XPS) on a Thermo Fisher ESCA-Lab250 spectrometer with a monochromatic Al Kα source. Acidity of samples were characterized by temperature-programmed desorption of ammonia (NH$_3$-TPD) using a Micromeritics AutoChem II 2920. The samples were heated to 600 °C in He atmosphere for 1 h, and then cooling to 100 °C. The system was switched to a mixture of 10% NH$_3$–He and the NH$_3$ was adsorbed until saturation for 1 h. Subsequently, the system was switched back to He and heated up to 600 °C again at a rate of 10 °C min^{-1}. The desorbed NH$_3$ was quantified by the thermal conductivity detector (TCD). The quantification of weakly acidic and strongly acidic sites was performed through the integration of NH$_3$-TPD curve and standard curve analysis.

Catalytic tests

All catalyst were supported with platinum using chloroplatinic acid as the precursor by the impregnation method, the content of the platinum was 0.5 mg per gram of catalyst. Subsequently, the catalyst was calcined at 450 °C under a hydrogen atmosphere for 3 h to obtain the reduced Pt/zeolite catalyst. The C_8 aromatics conversion was tested in a fixed bed reactor with an inner diameter of 6 mm and a length of 750 mm. Both the upper and lower catalysts were loaded at a weight of 0.3 g, resulting in a total catalyst loading of 0.6 g. The molar composition of the reaction mixture was $MX : OX : EB = 50 : 45 : 5$. The Weight Hourly Space Velocity (WHSV) was varied from $10\ h^{-1}$ to $20\ h^{-1}$ by adjusting the reactant flow rate. The reaction temperature and pressure were maintained at 380 °C and 1.0 MPa respectively. In order to ensure catalyst stability, a continuous injection of H_2 into the reactant was implemented, maintaining a molar ratio of H_2/Aromatics (H_2/C) at 1. The reaction product was analyzed by online gas phase chromatograph using Agilent 7890A which equipped with a HP-WAX column (60 m × 0.25 mm × 0.5 μm) and a FID detector.

The catalyst activity was determined by the ratio of PX in the product to the total xylene content (PX/X) and the EB conversion (EBC), which can be calculated using the following formula:

$$PX/X(\%) = W_{PX}/W_X \times 100$$

$$EBC(\%) = (W_{EBi} - W_{EBo})/W_{EBi} \times 100$$

where W_{PX} is the amount of PX in the product, W_X is the total amount of xylene in the product. Owing to the thermodynamic equilibrium limitation, the highest proportion of PX in xylene mixture is about 24%. W_{EBo} is the amount of EB in the product, W_{EBi} is the amount of EB in the reactant. The selectivity of the catalyst was determined by yield of xylene X_y, which was calculated by the ratio of the total xylene in the product to the total xylene in the reactant:

$$X_y(\%) = W_{Xo}/W_{Xi} \times 100$$

W_{Xo} is the total amount of xylene in the product, W_{Xi} is the total amount of xylene in the reactant.

Results and discussion

Characterization of the CLD samples

Fig. 1 shows the XRD pattern of each CLD sample. It is specified that the relative crystallinity of Z5 sample is 100%, and the relative crystallinity of Z5-S-(0.2–0.8) sample is 98%, 96%, 90% and 81%, respectively. As depicted in the figure, an increase in TEOS content in the solution does not alter the crystal structure of ZSM-5 zeolite, but leads to a slight decrease in zeolite crystallinity, probably due to the deposition of SiO_2 on its surface.

Fig. 2 shows the SEM images of Z5 and Z5-S-0.6 samples. It is evident from the figure that the crystal morphology of zeolite remained largely unchanged before and after modification. However, post-modification revealed a limited quantity of small
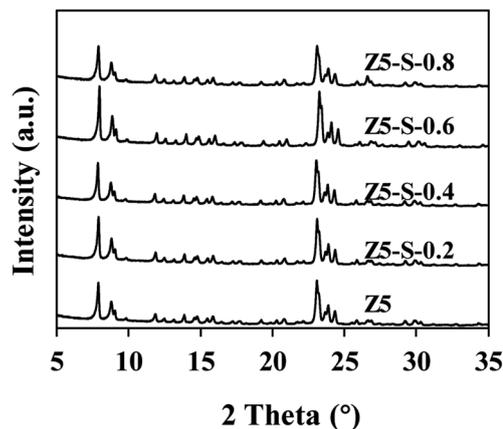

Fig. 1 XRD patterns of CLD samples.

particles on the crystal surface, and the crystal surface became rough, possibly attributed to the SiO_2 deposition.

The textural properties of each sample are summarized in Table 1. The bulk SiO_2/Al_2O_3 molar ratios were determined using XRF, while the surface SiO_2/Al_2O_3 molar ratios were determined using XPS. Analysis of the data presented in Table 1 reveals that with an increase in TEOS content in the solution, both the SiO_2/Al_2O_3 molar ratio of the bulk phase and the surface exhibit an upward trend. Notably, however, it is observed that the SiO_2/Al_2O_3 molar ratio of the surface demonstrates a more rapid increase compared to that of the bulk phase, indicating predominant deposition of SiO_2 on the outer surface. Additionally, a slight reduction is observed in both the specific surface area and pore volume of the CLD zeolite samples. This can be attributed to the limited penetration of TEOS into the pores of ZSM-5 zeolite due to its large size, resulting in predominant SiO_2 deposition on the external surface with minimal impact on the internal pore structure of the zeolite.

The NH_3-TPD curves of each CLD sample are presented in Fig. 3. It is evident that two distinct NH_3 desorption peaks appear near 200 °C and 400 °C, corresponding to weak acid sites and strong acid sites, respectively. The acid content was determined by integrating the area under the curve, and the results are summarized in Table 2. Remarkably, an increase in TEOS content leads to a gradual reduction in acid content within the samples. This can be attributed to the reaction between TEOS and acid sites on the exteral surface, resulting in SiO_2 coverage after calcining and subsequent passivation of these acidic sites. Consequently, there is a reduction in the overall quantity of acidic species present. However, it should be noted that this decrease is relatively minor overall, suggesting that SiO_2 deposition on the exteral surface has limited impact on the total acidity level within most pores.

Characterization of the ZSM-39 samples

The XRD pattern of the zeolite sample synthesized under different OH^-/SiO_2 molar ratios using pyrroliane as the SDA is presented in Fig. 4. It can be observed that at the OH^-/SiO_2 ratio of 0.07, the synthesized zeolite exhibits a ZSM-5 structure, while other samples show characteristic peaks corresponding to ZSM-
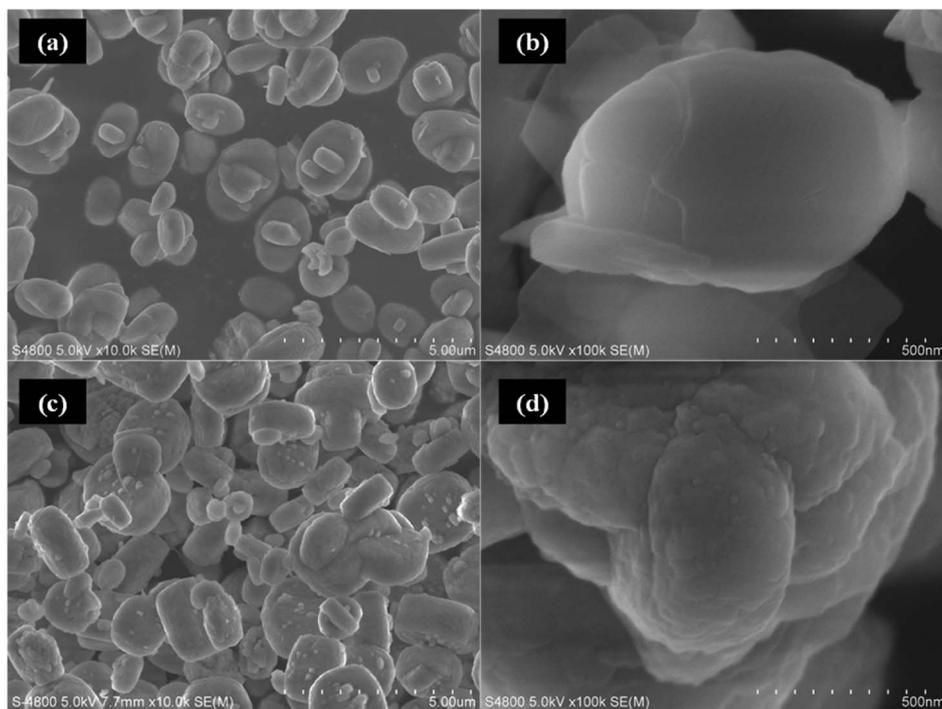
Fig. 2 SEM images of Z5 (a and b) and Z5-S-0.6 (c and d).

Table 1 Textural properties of the CLD samples

Samples	Bulk SiO_2/Al_2O_3	Surface SiO_2/Al_2O_3	Specific surface area/(m² g⁻¹)			Pore volume/(cm³ g⁻¹)		
			Total	Micro	Meso	Total	Micro	Meso
Z5	100	80	357.32	334.57	22.75	0.194	0.156	0.038
Z5-S-0.2	106	88	350.12	330.21	19.91	0.191	0.155	0.036
Z5-S-0.4	110	99	346.22	327.52	18.70	0.188	0.153	0.035
Z5-S-0.6	114	111	343.22	325.16	18.06	0.185	0.151	0.034
Z5-S-0.8	117	114	342.11	324.22	17.89	0.184	0.151	0.033

Fig. 3 NH₃-TPD curves of CLD samples.

Table 2 Acid properties of CLD samples

Samples	Acid amount (mmol g⁻¹)		
	Weak	Strong	Total
Z5	0.325	0.223	0.548
Z5-S-0.2	0.318	0.221	0.539
Z5-S-0.4	0.303	0.216	0.519
Z5-S-0.6	0.298	0.202	0.500
Z5-S-0.8	0.295	0.199	0.494

weak impure peaks appearing when the alkalinity is too low. Therefore, the optimal molar ratio for OH^-/SiO_2 synthesis is determined to be 0.05.

Fig. 5 shows the SEM image of PY-(0.01–0.05) sample. As depicted, when the OH^-/SiO_2 in the synthetic system is 0.01, numerous miscellaneous crystals are observed within the zeolite, and the individual particle size of the zeolite is larger, approximately 20 μm. By increasing the OH^-/SiO_2 ratio to 0.03
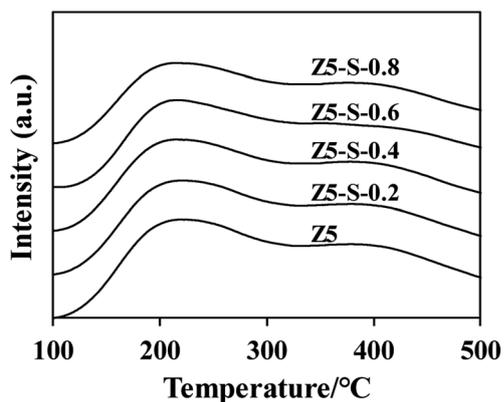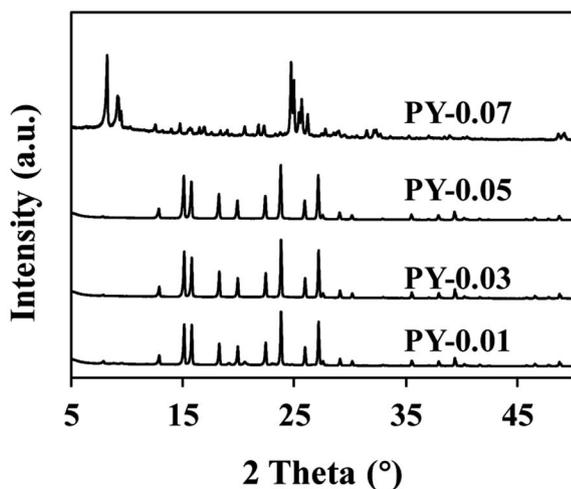
39 zeolite. This suggests that ZSM-39 synthesis requires lower alkalinity conditions. The relative crystallinity of PY-(0.01–0.05) samples is found to be 84%, 95%, and 100% respectively, with

Fig. 4 XRD patterns of PY-(0.01–0.07).

Table 3 Textural properties of PY-(0.01–0.05) samples

Samples	SiO_2/Al_2O_3	S_{total} (m² g⁻¹)	S_{micro} (m² g⁻¹)	V_{micro} (cm³ g⁻¹)
PY-0.01	96	158.33	156.32	0.087
PY-0.03	98	171.26	170.15	0.091
PY-0.05	100	194.88	194.21	0.093

The textural properties of PY-(0.01–0.05) samples are summarized in Table 3, and the SiO_2/Al_2O_3 ratio of the samples is determined by XRF analysis. The results indicate the absence of a mesoporous structure in the ZSM-39 samples. Among all samples, PY-0.05 exhibits the highest specific surface area and micropore volume. However, compared to the data of Z5 sample in Table 1, it is observed that both specific surface area and pore volume of PY-0.05 are significantly lower, which can be attributed to the larger crystal size of ZSM-39 zeolite.

The NH_3-TPD curve of ZSM-39 is presented in Fig. 6, revealing desorption peaks around 200 °C and 450 °C, corresponding to weak acid centers and strong acid centers, respectively. Table 4 displays the acid content of each sample.

and 0.05, uniform particles of ZSM-39 zeolite can be obtained with smaller particle sizes around 10 μm being achieved specifically at the OH^-/SiO_2 ratio of 0.05.
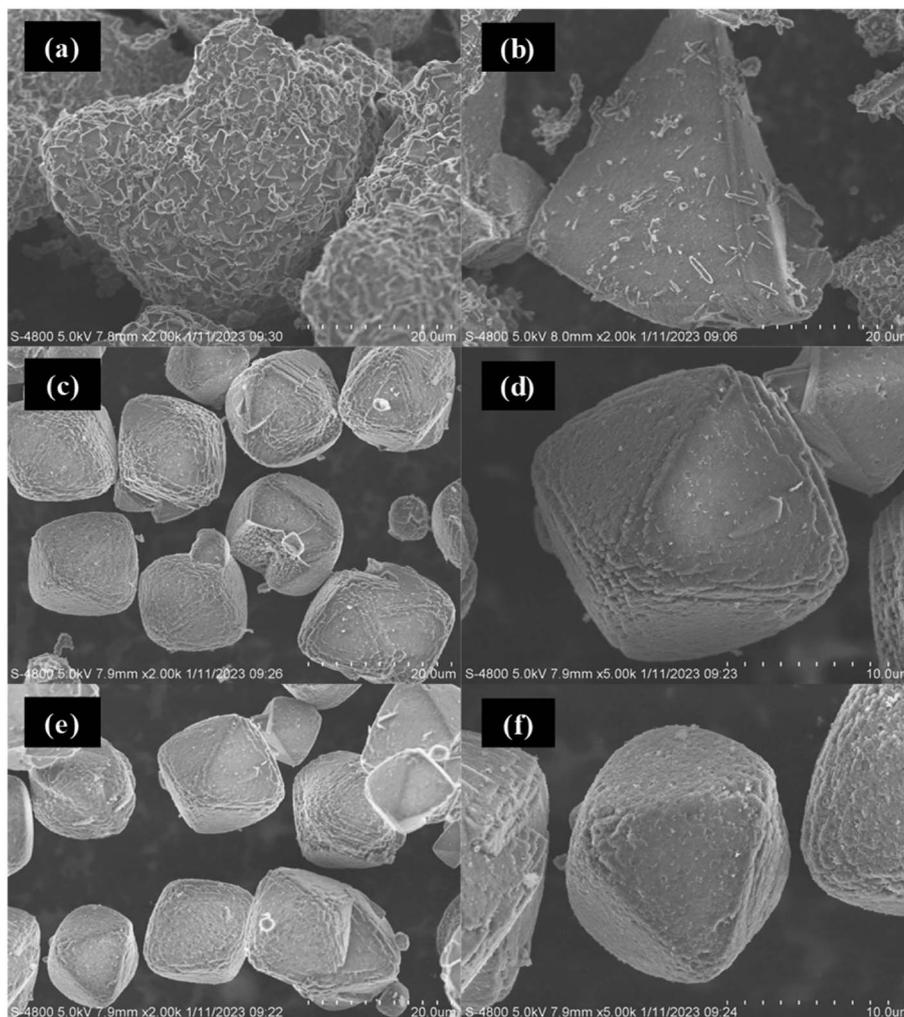

Fig. 5 SEM images of PY-0.01 (a and b), PY-0.03 (c and d), PY-0.05 (e and f).
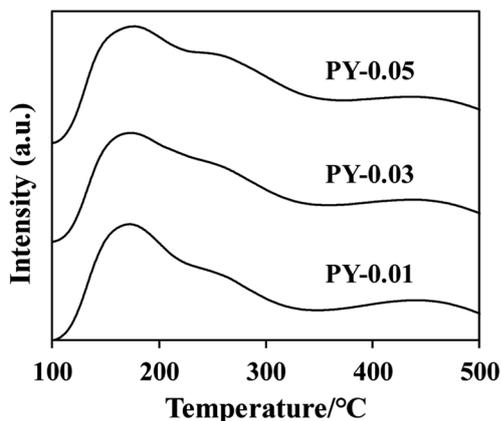
Fig. 6 NH$_3$-TPD curves of PY-(0.01–0.05).

Table 4 Acid properties of PY-(0.01–0.05)

Samples	Acid amount (mmol g^{-1})		
	Weak	Strong	Total
PY-0.01	0.259	0.162	0.421
PY-0.03	0.263	0.168	0.431
PY-0.05	0.286	0.176	0.462

Notably, the PY-0.05 sample exhibits the highest apparent acid content, slightly lower than that of the Z5 sample in Table 2. This discrepancy may be attributed to the restricted accessibility of NH$_3$ molecules to acidic sites within the small pore size of ZSM-39 zeolite.

Catalytic performance on C$_8$ aromatics conversion

The catalytic performance of Z5, Z5-S-(0.2–0.8), and PY-(0.01–0.05) catalysts was evaluated under the conditions of a temperature of 380 °C, pressure of 1.0 MPa, WHSV of 20 h^{-1}, H$_2$/C of 1, with a catalyst loading of 0.3 g. The results are presented in Fig. 7. The isomerization activity of xylene gradually decreases with the increase in the amount of TEOS added, as observed from Fig. 7 (a–c), indicating that SiO$_2$ covers the acidic sites on the external surface of the catalyst. When the amount of TEOS is less than 0.6 mL g^{-1}, there is a gradual increase in EBC due to the small molecular size of EB and PX, enabling their free entry and exit through ZSM-5 pores. Consequently, EB deethylation reaction predominantly occurs within ZSM-5 pores. As the generation of PX decreases, its influence on EB diffusion within ZSM-5 pores weakens leading to an increased EBC. When the addition amount of TEOS is 0.8 mL, the conversion rate of ethylbenzene decreases due to excessive SiO$_2$ deposition, hindering EB from entering the ZSM-5 pores and resulting in a reduced conversion rate of ethylbenzene. Therefore, based on comprehensive results, Z5-S-0.6 emerges as the optimal upper catalyst.

The xylene isomerization activity and ethylbenzene deethylation activity of ZSM-39 increased with the increase in OH$^-$/SiO$_2$, as observed from Fig. 7 (d–f). Although there was a slight decrease in xylene yield, it remained above 99%. Therefore, PY-0.05 was selected as the lower catalyst. Compared with the evaluation results of the Z5 and PY-0.05 samples, it was observed that the xylene isomerization activity of the Z5 sample exhibited minimal variation, while the EBC value was high. Conversely, the X$_y$ value of the PY-0.05 sample was high. The pore orifice of ZSM-39 exclusively consists of six-membered rings, thereby preventing the entry of OX and MX molecules. Consequently, xylene isomerization can only take place on the external surface of ZSM-39 zeolite. Although the molecular sizes of OX and MX are similar to the pore sizes of ZSM-5, their diffusion within the pores is hindered due to size constraints. Hence, it is postulated that xylene isomerization also occurs predominantly on the outer surface of ZSM-5, resulting in
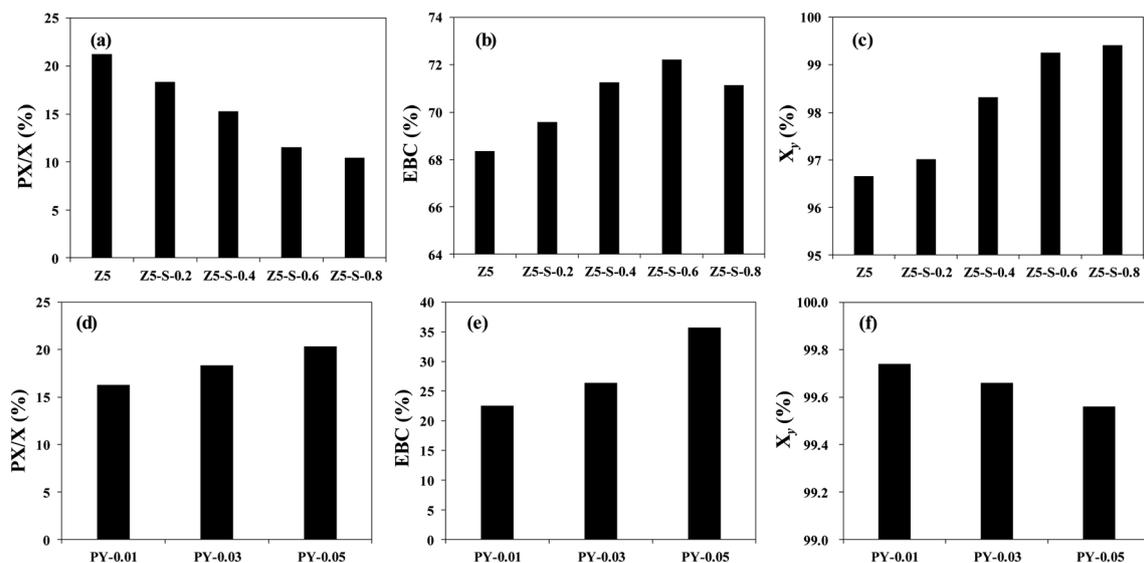

Fig. 7 Catalytic performance of C$_8$ conversion on Z5, Z5-S-(0.2–0.8) (a–c), and PY-(0.01–0.05) (d–f). Reaction conditions: T = 380 °C, P = 1 MPa, WHSV = 20 h^{-1}, H$_2$/C = 1.

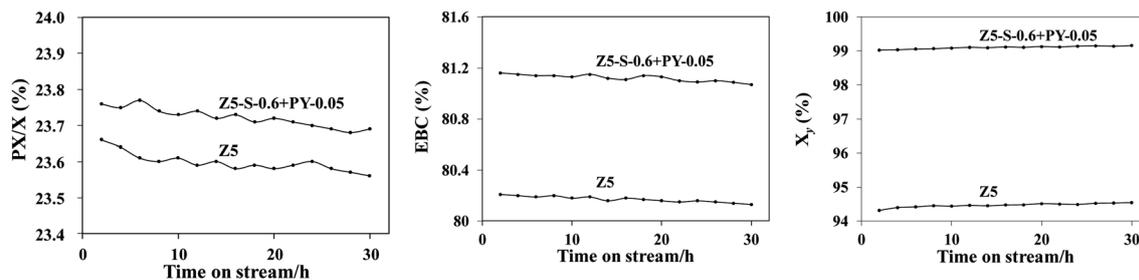**Fig. 8** Catalytic performance of C_8 conversion on dual bed catalyst and Z5 sample. Reaction conditions: $T = 380$ °C, $P = 1$ MPa, WHSV $= 10$ h^{-1}, $H_2/C = 1$.

minimal disparity in xylene isomerization activities between ZSM-5 and ZSM-39. Ethylbenzene cannot permeate into the pores of ZSM-39; however, it can freely access those within ZSM-5, leading to significantly higher ethylbenzene conversion in comparison with that observed for ZSM-39. Xylene disproportionation emerges as a prominent side reaction during C_8 aromatic conversion processes. Given its bimolecular nature, two para-xylene molecules are more likely to encounter each other within the pore channels of ZSM-5. Consequently, an elevated propensity for side reactions exists in relation to ZSM-5 catalysts.

The lower layer was loaded with 0.3 g of PY-0.05 catalyst, while the upper layer contained 0.3 g of Z5-S-0.6 catalyst. Catalytic performance was evaluated at a temperature of 380 °C, pressure of 1 MPa, H_2/C of 1, and overall WHSV of 10 h^{-1}. For comparison purposes, catalytic performance was also assessed using a single-layer Z5 sample loaded with 0.6 g under identical conditions, as depicted in Fig. 8. It is evident that both catalysts exhibit good stability, and the dual bed catalyst demonstrates higher activity and selectivity compared to the single-layer ZSM-5 catalyst.

Conclusions

A dual-bed catalyst for conversion of C_8 aromatics was prepared. The upper layer catalyst was prepared mainly for EB deethylation. The CLD method was employed to load SiO_2 on the surface of the catalyst, which effectively passivated the acid sites on the outer surface and inhibited the conversion of o-xylene and m-xylene to p-xylene. By reducing the production of p-xylene in the upper layer, it minimized its influence on EB diffusion within pores, leading to an increased conversion rate of EB. It was observed that when 0.6 mL TEOS deposition agent per gram of catalyst was used, the highest ethylbenzene conversion in the upper layer was achieved. For xylene isomerization, ZSM-5 and ZSM-39 were utilized as catalysts primarily acting on their outer surfaces. However, due to its inability to enter into ZSM-39 pores, p-xylene exhibited a significantly lower bimolecular reaction rate compared to ZSM-5. Consequently, ZSM-39 demonstrated excellent selectivity in xylene isomerization reactions. Therefore, ZSM-39 was chosen as the catalyst for the lower layer. The dual-bed catalyst consisting of equal mass ratios between upper and lower layers exhibited higher activity and selectivity than the traditional single-layer ZSM-5 catalysts.

Conflicts of interest

There are no conflicts to declare.

Acknowledgements

Notes and references

1 Q. Shi, J. C. Gonçalves, A. F. Ferreira and A. E. Rodrigues, *Chem. Eng. Process.*, 2021, **169**, 108603.
2 C. Fernandez, I. Stan, J. P. Gilson, K. Thomas, A. Vicente, A. Bonilla and J. Pérez Ramírez, *Chem.–Eur. J.*, 2010, **16**, 6224–6233.
3 D. I. Collias, A. M. Harris, V. Nagpal, I. W. Cottrell and M. W. Schultheis, *Ind. Biotechnol.*, 2014, **10**, 91–105.
4 R. D. Chirico, S. E. Knipmeyer, A. Nguyen and W. V. Steele, *J. Chem. Eng. Data*, 1997, **42**, 248–261.
5 R. D. Chirico, S. E. Knipmeyer, A. Nguyen, J. W. Reynolds and W. V. Steele, *J. Chem. Eng. Data*, 1997, **42**, 475–487.
6 M. Minceva, P. S. Gomes, V. Meshko and A. E. Rodrigues, *Chem. Eng. J.*, 2008, **140**, 305–323.
7 Y. Yang, P. Bai and X. Guo, *Ind. Eng. Chem. Res.*, 2017, **56**, 14725–14753.
8 K. Santos, A. D. Neto, M. Moura and T. C. Dantas, *Braz. J. Pet. Gas*, 2011, **5**, DOI: **10.5419/bjpg2011-0024**.
9 G. Xomeritakis, Z. Lai and M. Tsapatsis, *Ind. Eng. Chem. Res.*, 2001, **40**, 544–552.
10 K. Toch, J. W. Thybaut, B. D. Vandegehuchte, C. Narasimhan, L. Domokos and G. B. Marin, *Appl. Catal., A*, 2012, **425**, 130–144.
11 N. R. Demikhova, M. I. Rubtsova, V. A. Vinokurov and A. P. Glotov, *Pet. Chem.*, 2021, **61**, 1158–1177.
12 C. Hu, J. Li, W. Jia, M. Liu, Z. Hao and Z. Zhu, *Chin. J. Chem.*, 2015, **33**, 247–252.
13 A. Iliyas and S. Al-Khattaf, *Ind. Eng. Chem. Res.*, 2004, **43**, 1349–1358.
14 A. Iliyas and S. Al-Khattaf, *Chem. Eng. J.*, 2005, **107**, 127–132.
15 A. M. Tarditi, S. Irusta and E. A. Lombardo, *Chem. Eng. J.*, 2006, **122**, 167–174.

16 J. Hao, P. Feng, F. Xin, Z. Wang, Z. Zhou, D. Bao and Z. Zhu, *Chem. Eng. Sci.*, 2023, **268**, 118425.

17 D. J. Collins, K. J. Mulrooney, R. J. Medina and B. H. Davis, *J. Catal.*, 1982, **75**, 291–301.

18 H. Min, S. H. Cha and S. B. Hong, *ACS Catal.*, 2012, **2**, 971–981.

19 M. Guisnet and N. S. Gnep, in *Zeolites: Science and Technology*, Springer, 1984, pp. 571–582.

20 A. Corma and E. Sastre, *J. Catal.*, 1991, **129**, 177–185.

21 A. M. Tarditi, G. I. Horowitz and E. A. Lombardo, *Catal. Lett.*, 2008, **123**, 7–15.

22 X. Chang, Y. Li and Z. Zeng, *Ind. Eng. Chem. Res.*, 1992, **31**, 187–192.

23 M. Kazemi, M. Emami Meibodi and S. H. Esmaeili-Faraj, *J. Appl. Res. Chem. Polym. Eng.*, 2023, **6**, 43–56.

24 M. Rasouli, H. Atashi, D. Mohebbi-Kalhori and N. Yaghobi, *J. Taiwan Inst. Chem. Eng.*, 2017, **78**, 438–446.

25 L. Miao, Z. Hong, X. Wang, W. Jia, G. Zhao, Y. Huang and Z. Zhu, *Microporous Mesoporous Mater.*, 2022, **332**, 111718.

26 P. Tamizhdurai, P. S. Krishnan, A. Ramesh and K. Shanthi, *Polyhedron*, 2018, **154**, 314–324.

27 Y. F. Chu, C. T. Kresge and R. B. LaPierre, *US Pat.*, 4899011, 1990.

28 D. L. Stern, *US Pat.*, 7247762B2, 2007.

29 G. D. Pirngruber, C. Laroche, M. Maricar-Pichon, L. Rouleau, Y. Bouizi and V. Valtchev, *Microporous Mesoporous Mater.*, 2013, **169**, 212–217.

30 D. Van Vu, M. Miyamoto, N. Nishiyama, S. Ichikawa, Y. Egashira and K. Ueyama, *Microporous Mesoporous Mater.*, 2008, **115**, 106–112.

31 A. Ghorbanpour, A. Gumidyala, L. C. Grabow, S. P. Crossley and J. D. Rimer, *ACS Nano*, 2015, **9**, 4006–4016.

32 T. Hui, W. Jun, R. Xiaoqian and C. Demin, *Chin. J. Chem. Eng.*, 2011, **19**, 292–298.

33 S. Zheng, H. R. Heydenrych, H. P. Röger, A. Jentys and J. A. Lercher, *Top. Catal.*, 2003, **22**, 101–106.

34 H. Manstein, K. P. Möller, W. Böhringer and C. T. O'Connor, *Microporous Mesoporous Mater.*, 2002, **51**, 35–42.

35 Y. Yue, Y. Tang, Y. Liu and Z. Gao, *Ind. Eng. Chem. Res.*, 1996, **35**, 430–433.

36 P. Losch, M. Boltz, C. Bernardon, B. Louis, A. Palčić and V. Valtchev, *Appl. Catal., A*, 2016, **509**, 30–37.

37 F. G. Dwyer and E. E. Jenkins, *US Pat.*, 4287166, 1981.

38 B. P. Pelrine, *US Pat.*, 4259306, 1981.

39 F. G. Dwyer and E. E. Jenkins, *US Pat.*, 4357233, 1982.

40 J. L. Schlenker, F. G. Dwyer, E. E. Jenkins, W. J. Rohrbaugh, G. T. Kokotailo and W. M. Meier, *Nature*, 1981, **294**, 340–342.

41 Z. S. Lin, D. Chen, H. Nie, Y. A. Wong and Y. Huang, *Can. J. Chem.*, 2019, **97**, 840–847.

42 D. M. Bibby and L. M. Parker, *Zeolites*, 1983, **3**, 11–12.

43 B. P. Pelrine, *US Pat.*, 4395327, 1983.